

KENNICUTT-SCHMIDT RELATION VARIETY AND STAR-FORMING CLOUD FRACTION

KANA MOROKUMA-MATSUI¹ AND KAZUYUKI MURAOKA²*Not to appear in Nonlearned J., 45.*

ABSTRACT

The observationally derived Kennicutt-Schmidt (KS) relation slopes differ from study to study, ranging from sub-linear to super-linear. We investigate the KS-relation variety (slope and normalization) as a function of integrated intensity ratio, $R_{31} = \text{CO}(J = 3 - 2)/\text{CO}(J = 1 - 0)$ using spatially resolved CO($J = 1 - 0$), CO($J = 3 - 2$), H I, H α and 24 μm data of three nearby spiral galaxies (NGC 3627, NGC 5055 and M 83). We find that (1) the slopes for each subsample with a fixed R_{31} are shallower but the slope for all datasets combined becomes steeper, (2) normalizations for high R_{31} subsamples tend to be high, (3) R_{31} correlates with star-formation efficiency, thus the KS relation depends on the distribution in R_{31} - Σ_{gas} space of the samples: no Σ_{gas} dependence of R_{31} results in a linear slope of the KS relation whereas a positive correlation between Σ_{gas} and R_{31} results in a super-linear slope of the KS relation, and (4) R_{31} - Σ_{gas} distributions are different from galaxy to galaxy and within a galaxy: galaxies with prominent galactic structure tend to have large R_{31} and Σ_{gas} . Our results suggest that the formation efficiency of star-forming cloud from molecular gas is different among galaxies as well as within a galaxy and is one of the key factors inducing the variety in galactic KS relation.

Subject headings: galaxies: evolution — galaxies: star formation — galaxies: ISM — galaxies: individual (M 83, NGC 3627, NGC 5055)

1. INTRODUCTION

Star formation is one of the essential processes of galaxy evolution. However, the physics of star formation is not fully understood because one must consider a large dynamic range of spatial scale as well as time scale, from kilo-parsec to 0.1 parsec and from Giga-year to Mega-year, respectively.

Schmidt (1959) first proposed a star formation model by assuming that the volume density of the star-formation rate ($\dot{\rho}_\star$) varies with a power n of the volume density of gas (ρ_{gas}) as $\dot{\rho}_\star \propto \rho_{\text{gas}}^n$. Thirty years later, Kennicutt (1989) observationally showed a strong relation between the surface densities of star formation rate (SFR), Σ_{SFR} , and cold gas mass, Σ_{gas} , inferred from the H I and CO($J = 1 - 0$) (hereafter, CO(1-0)) luminosities of nearby galaxies: $\Sigma_{\text{SFR}} \propto \Sigma_{\text{gas}}^{1.4}$. In a more general form that incorporates a power of N , the relation $\Sigma_{\text{SFR}} \propto \Sigma_{\text{gas}}^N$ is referred to as the Kennicutt-Schmidt (KS) relation.

Since the proposition of the KS relation, various studies have reported various normalizations and slopes of the KS relation mainly based on molecular gas (hereafter molecular KS relation), – i.e., $\Sigma_{\text{gas}} \propto \Sigma_{\text{mol}}^N$, where Σ_{mol} is molecular gas surface density. For example, higher normalizations are suggested for starbursts (e.g., Daddi et al. 2010) and smaller normalizations for early-type galaxies (e.g., Martig et al. 2013) compared to normal disk galaxies. Even for the normal disk galaxies, various slopes are reported including sub-linear (e.g., Shetty et al. 2013), linear (e.g., Bigiel et al. 2008), and super-linear (e.g., Momose et al. 2013). Many studies

suggested that the variation is due to the differences in methodology such as SFR estimation (Liu et al. 2011; Momose et al. 2013, see also Rahman et al. 2011, 2012), molecular gas mass estimation (Momose et al. 2013), fitting method (e.g., Blanc et al. 2009; Verley et al. 2010), and spatial resolution of the data (Kennicutt et al. 2007; Thilker et al. 2007; Onodera et al. 2010; Momose et al. 2010; Liu et al. 2011; Calzetti et al. 2012).

Some studies suggested that the reported KS-relation variety is not only due to different methodologies but also genuine and intrinsic. Lada et al. (2012) explicitly showed that the Milky Way molecular clouds and nearby galaxies with the same dense core gas fraction follow the same linear molecular KS relation and that the normalizations tend to be high for systems with high dense core gas fraction. This is based on the observational result that SFR correlates linearly with dense core mass (traced by HCN) in molecular clouds and galaxies (Solomon et al. 1992; Gao & Solomon 2004a,b; Wu et al. 2005). As a subsequent step, we must investigate the controlling factors of dense core gas fractions in various galactic environments and galaxies. However, previous HCN observations were mainly conducted toward the centers of nearby galaxies, and only a few galaxies have been mapped recently, since the HCN emission is generally 10 – 30 times weaker than CO (M82: Kepley et al. 2014, Antennae: Bigiel et al. 2015, M51: Chen et al. 2015; Bigiel et al. 2016).

It has been shown that line luminosities of the high- J transitions of CO, the second most abundant molecule, also linearly correlate with SFR (or infrared luminosity) (Liu et al. 2015, see also Bayet et al. 2009; Greve et al. 2014). Especially, CO($J = 3 - 2$) (hereafter, CO(3-2)) mapping observations were conducted toward a number of galaxies (e.g., Wilson et al. 2009) with observational indication that CO(3-2) correlates linearly with

kana.matsui@nao.ac.jp

¹ Chile Observatory, National Astronomical Observatory of Japan, 2-21-1 Osawa, Mitaka-shi, Tokyo 181-8588, Japan² Department of Physical Science, Osaka Prefecture University, 1-1 Gakuen-cho, Naka-ku, Sakai, Osaka 599-8531, Japan

SFR over four orders of magnitudes (Narayanan et al. 2005; Komugi et al. 2007; Bayet et al. 2009; Iono et al. 2009; Mao et al. 2010; Greve et al. 2014; Muraoka et al. 2016). Although CO(3-2) emission is likely to be optically thick toward the dense cores, CO(3-2) traces dense ($\sim 10^4 \text{ cm}^{-3}$) and warm (30 – 50 K) gas, which is found around cores heated by star formation (e.g. Minamidani et al. 2008; Kawamura et al. 2009; Dempsey et al. 2013; Miura et al. 2014). In addition, CO(3-2) is considered to be an indicator of the early stage star formation, since it also traces outflows from protostars (e.g. van Kempen et al. 2006; Su et al. 2007; Takahashi et al. 2008).

In this study, we investigate the relationship between the variety in the CO(3-2)/CO(1-0) ratio of nearby spiral galaxies and the resultant slopes of the KS relation. We consider the CO(3-2)/CO(1-0) ratio as a measure of star-forming gas fraction. The structure of this paper is as follows; we first describe the observational data in Section 2. Then we show the variety in the CO(3-2)/CO(1-0) ratios within a galaxy and among galaxies, and how the KS-relation slope depends on the CO(3-2)/CO(1-0) ratio in Section 3. We propose “hierarchical KS relation” and discuss which hierarchical steps of interstellar medium (ISM) impose a variety in the KS relation and what controls the ISM hierarchy balance in disk galaxies in Section 4.

2. DATA

A summary of the observational data used in this study is given in Table 1. All three galaxies are nearby late-type galaxies with grand design (NGC 3627 and M 83) or flocculent (NGC 5055) spiral structures (Elmegreen & Elmegreen 1987). They belong to a similar population of galaxies in terms of stellar mass and SFR plane (Figure 1) but NGC 3627 seems to have lower metallicity than the other two galaxies (Figure 2). We use archival data to estimate gas and SFR surface densities. The spatial resolutions of the data are 15 arcsec for NGC 3627 (700 pc at the distance of the galaxy) and NGC 5055 (570 pc), and 25 arcsec for M 83 (550 pc). The inclination corrected spatial resolutions are 892 pc for NGC 3627, 819 pc for NGC 5055, and 575 pc for M 83, which are larger than the boundary spatial resolutions at which the KS relation breaks (80 – 250 pc, Momose et al. 2010; Verley et al. 2010; Onodera et al. 2010). In the following subsections, we briefly summarize the data and derivations of the physical values such as total cold gas mass and SFR from the observed quantities.

2.1. Gas surface density and CO(3-2)/CO(1-0) ratio

The estimation of gas surface density (Σ_{gas}) requires data on the H_2 and H I column densities. Here, the estimate of Σ_{gas} takes into account He content (multiplied with a factor of 1.36, based on the (proto-) Solar abundance, e.g., Asplund et al. 2009). CO(1-0) data for our sample of galaxies were obtained with the 45-m telescope as a part of Nobeyama CO Atlas survey (Kuno et al. 2007). We adopt a CO-to- H_2 conversion factor of $X_{\text{CO}} = 1.8 \times 10^{20} \text{ cm}^{-2} (\text{K km s}^{-1} \text{ pc}^2)^{-1}$ to estimate the H_2 column density from the CO integrated intensity (Dame et al. 2001). H I data were obtained with Very Large Array (VLA) as a part of The H I Nearby

Galaxy Survey (THINGS, Walter et al. 2008). The H I column density is estimated according to Equation (5) of Walter et al. (2008). The sensitivity of Σ_{gas} is $32 \text{ M}_{\odot} \text{ pc}^{-2}$ for NGC 3627, $11 \text{ M}_{\odot} \text{ pc}^{-2}$ for NGC 5055, and $30 \text{ M}_{\odot} \text{ pc}^{-2}$ for M 83.

The integrated intensity CO(3-2)/CO(1-0) ratio is defined as,

$$R_{31} = \frac{I_{\text{CO}(3-2)}}{I_{\text{CO}(1-0)}}, \quad (1)$$

where $I_{\text{CO}(3-2)}$ and $I_{\text{CO}(1-0)}$ are integrated intensities of CO(3-2) and CO(1-0), respectively. CO(3-2) data were obtained with the Atacama Submillimeter Telescope Experiment (ASTE) telescope for M 83 (Muraoka et al. 2009) and with the James Clerk Maxwell Telescope (JCMT) for NGC 3627 and NGC 5055 as a part of the JCMT Nearby Galaxies Legacy Survey (NGLS, Wilson et al. 2012).

2.2. SFR surface density

We combined $\text{H}\alpha$ and $24 \mu\text{m}$ data to estimate dust extinction-corrected $\text{H}\alpha$ luminosity using to Equation (5) of Calzetti et al. (2007)³. Then, SFR surface density (Σ_{SFR}) is estimated from the $\text{H}\alpha$ luminosity according to Equation (2) of Kennicutt (1998). $\text{H}\alpha$ and $24 \mu\text{m}$ data are retrieved from the SIRTf Nearby Galaxies Survey (SINGS, Kennicutt et al. 2003) for NGC 3627 and the Spitzer Local Volume Legacy (LVL, Dale et al. 2009) for NGC 5055 and M 83, respectively. [NII] contribution to $\text{H}\alpha$ luminosity was subtracted for all the data.

3. RESULTS

3.1. Spatial distribution of CO(3-2)/CO(1-0)

Figures 3, 4 and 5 respectively show Σ_{gas} , R_{31} and star formation efficiency ($\text{SFE} = \Sigma_{\text{SFR}}/\Sigma_{\text{gas}}$) maps of the sample galaxies. The intensity scales for each figure were set to be the same. The Σ_{gas} distributions are shown in all the maps as white contours as references. The outermost contours in Figures 3, 4 and 5 correspond to the Σ_{gas} sensitivities of each galaxy. Σ_{gas} is high at the central regions of all the sample galaxies and at the bar regions, especially the bar-end regions of NGC 3627 and M 83, as shown in Figure 3. The spiral arm structures can be also seen in the Σ_{gas} maps of NGC 3627 and M 83. For the R_{31} and SFE maps, the overall trends resemble each other: high values at downstreams of the bar-end regions and central regions.

3.2. CO(3-2)/CO(1-0) ratio and the KS-relation

Figure 6 shows $\Sigma_{\text{SFR}} - \Sigma_{\text{gas}}$ relation (KS relation), CO(1-0)-based and CO(3-2)-based molecular KS relations: molecular gas surface densities, $\Sigma_{\text{mol,CO}(1-0)}$ and $\Sigma_{\text{mol,CO}(3-2)}$ are inferred from CO(1-0) and CO(3-2) integrated intensities, respectively. $\Sigma_{\text{mol,CO}(3-2)}$ is converted from CO(3-2) integrated intensity by assuming the same X_{CO} for CO(1-0) without CO(3-2)-to-CO(1-0) conversion. The KS-relation slopes were derived using ordinary least-squares (OLS) regression of

³ The diffuse emission of $\text{H}\alpha$ and $24 \mu\text{m}$ was not extracted, although it can also affect the slope of KS relation (Liu et al. 2011). The effect of the diffuse emission on SFR estimation and our results is discussed in Appendix.

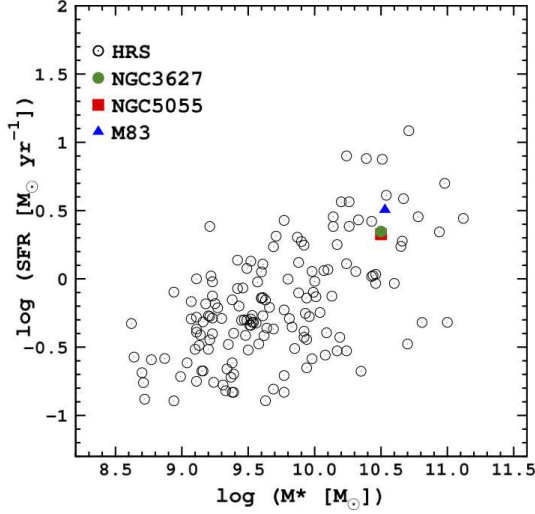


FIG. 1.— Stellar mass and SFR relation of nearby galaxies including NGC 3627 (green circle), NGC 5055 (red square) and M 83 (blue triangle). Stellar masses based on 3.6 μ m and SFRs of both NGC 3627 and NGC 5055 are retrieved from Leroy et al. (2013) and Leroy et al. (2008), respectively. Stellar mass and SFR of M 83 are retrieved from Jarrett et al. (2013). The black-filled circle indicates the galaxies from Herschel Reference Survey (HRS, Boselli et al. 2010) as a reference; stellar mass based on i -band luminosity and $g - i$ color from Cortese et al. (2012), and SFR based on FUV and 24 μ m luminosity from Boselli et al. (2015). The sample galaxies are on the star-forming *main-sequence* and located closely.

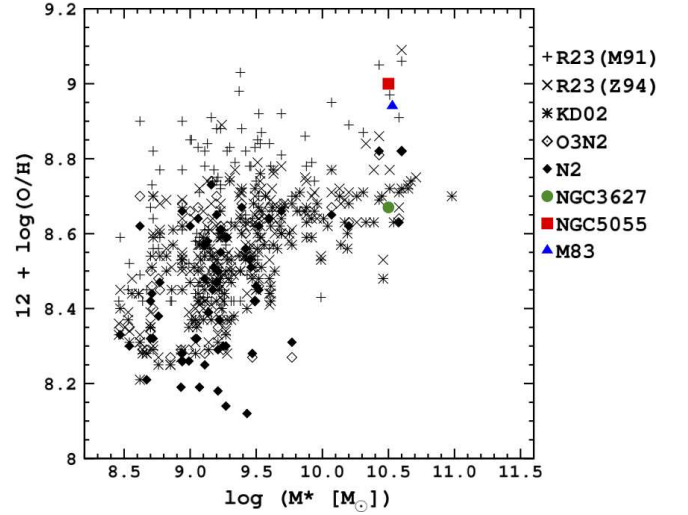


FIG. 2.— Stellar mass and metallicity relation of nearby galaxies including NGC 3627 (green circle), NGC 5055 (red square) and M 83 (blue triangle). Metallicities based on R23 calibration with Kobulnicky & Kewley (2004) (KK04) and Pilyugin & Thuan (2005) (PT05) of NGC 3627 and NGC 5055 are retrieved from Moustakas et al. (2010). Averaged values at the galactic center of PT05 and KK04 calibrations are adopted (Table. 9 of Moustakas et al. (2010)). Direct measurement of metallicity at the center of M 83 based on electric temperature is retrieved from Bresolin et al. (2005). Black symbols indicate HRS galaxies and the metallicities of them are retrieved from Hughes et al. (2013); cross, R23 calibration based on McGaugh (1991); x, R23 calibration based on Zaritsky et al. (1994); asterisk, [Nii] λ 6584/[Oii] λ 3727 calibration based on Kewley & Dopita (2002); open diamond, O3N2 calibration based on Pettini & Pagel (2004); filled diamond, N2 calibration based on Pettini & Pagel (2004). Metallicities of NGC 5055 and M 83 seem higher than that of NGC 3627 even considering the difference in the calibration methods.

TABLE 1
SUMMARY OF THE OBSERVATIONAL DATA USED IN THIS STUDY

Galaxy	Type (RC3)	Arm class ^a	Dist. (ref.) ^b (Mpc)	i (ref.) ^c (deg)	Resolution ^d (pc)	CO(1-0)	CO(3-2)	H I	SFR
NGC 3627	SAB(s)b	7	11.1 (1)	52 (1)	892	NRO45	JCMT	THINGS	SINGS
NGC 5055	SA(rs)bc	3	7.2 (2)	61 (1)	819	NRO45	JCMT	THINGS	LVL
M 83	SAB(s)c	9	4.5 (3)	24 (2)	575	NRO45	ASTE	THINGS	LVL

NOTE. — ^a 7 and 9 indicate a grand design spiral and 3 indicates a flocculent (Elmegreen & Elmegreen 1987).

^b References of distance. 1: Saha et al. (1999), 2: Pierce (1994), 3: Thim et al. (2003)

^c References of inclination. 1: Kuno et al. (2007), 2: Comte (1981)

^d i -corrected resolution.

Σ_{SFR} on Σ_{gas} , $\text{OLS}(\Sigma_{\text{SFR}}|\Sigma_{\text{gas}})$, and the bisector of $\text{OLS}(\Sigma_{\text{SFR}}|\Sigma_{\text{gas}})$ and $\text{OLS}(\Sigma_{\text{gas}}|\Sigma_{\text{SFR}})$. The slope of CO(3-2)-based molecular KS relation is linear whereas the CO(1-0)-based one is super-linear in both the fitting methods, suggesting the difficulty in deriving molecular KS relation from CO(3-2) with a fixed CO(3-2)-to-CO(1-0) conversion factor. As previous studies have shown, the slope of the bisector of the two OLSs is steeper than that of $\text{OLS}(\Sigma_{\text{SFR}}|\Sigma_{\text{gas}})$ (e.g., Isobe et al. 1990). A tighter relation for CO(3-2)-based molecular KS relation than CO(1-0)-based one indicates that CO(3-2) traces molecular gas that is more closely related to star formation. We only used pixels for which CO(1-0), CO(3-2) and H I were detected. Therefore, the area we studied here is somehow biased to molecular-dominated regions: all data points have $\text{H}_2/\text{H I} > 1$.

Figure 7 shows the KS relation of NGC 3627,

NGC 5055, and M 83. KS relation plots are divided into subsamples based on the R_{31} values – these are color-coded according to R_{31} in Figure 7. The slopes of the KS relations for each sub-sample of R_{31} are shallower than that obtained when fitting to all data concurrently. The normalization for higher- R_{31} subsamples tend to be higher than those for the lower- R_{31} subsamples (see Table 2). These trends are independent of the fitting methods: $\text{OLS}(\Sigma_{\text{SFR}}|\Sigma_{\text{gas}})$ or a bisector of $\text{OLS}(\Sigma_{\text{SFR}}|\Sigma_{\text{gas}})$ and $\text{OLS}(\Sigma_{\text{gas}}|\Sigma_{\text{SFR}})$. This trend is still seen even if we use Σ_{mol} instead of Σ_{gas} . We emphasize here that the different galaxies follow the same $\Sigma_{\text{SFR}}/\Sigma_{\text{gas}}$ relations for each R_{31} even though data were not all obtained in the same conditions (observing seasons and instruments used). This trend suggests that R_{31} is correlated with the $\Sigma_{\text{SFR}}/\Sigma_{\text{gas}}$ ratio – i.e., SFE. Indeed, Figure 8 shows a clear correlation between R_{31} and SFE. In this plot,

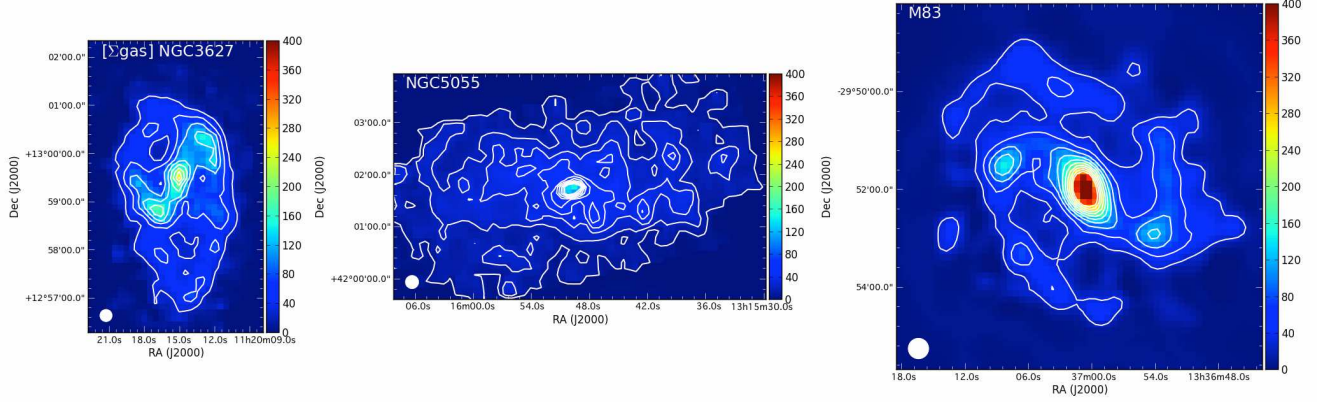


FIG. 3.— Σ_{gas} ($M_{\odot} \text{ pc}^{-2}$) maps of the sample galaxies. Intensity scales are set to be identical among the galaxies. The unit for the color bar is $M_{\odot} \text{ pc}^{-2}$. The spatial resolutions are shown on the bottom-left corner of each plot. The pixel sizes are set to 7.3 arcsec for NGC 3627, 7.0 arcsec for NGC 5055 and 7.5 arcsec for M 83. White contours trace the distribution of Σ_{gas} with contour levels of 1σ , 2σ , 3σ , 4σ , 5σ , 6σ , 7σ , 8σ , 9σ , 10σ . 1σ s for NGC 3627, NGC 5055, M 83 are 32, 11, and 30 $M_{\odot} \text{ pc}^{-2}$, respectively.

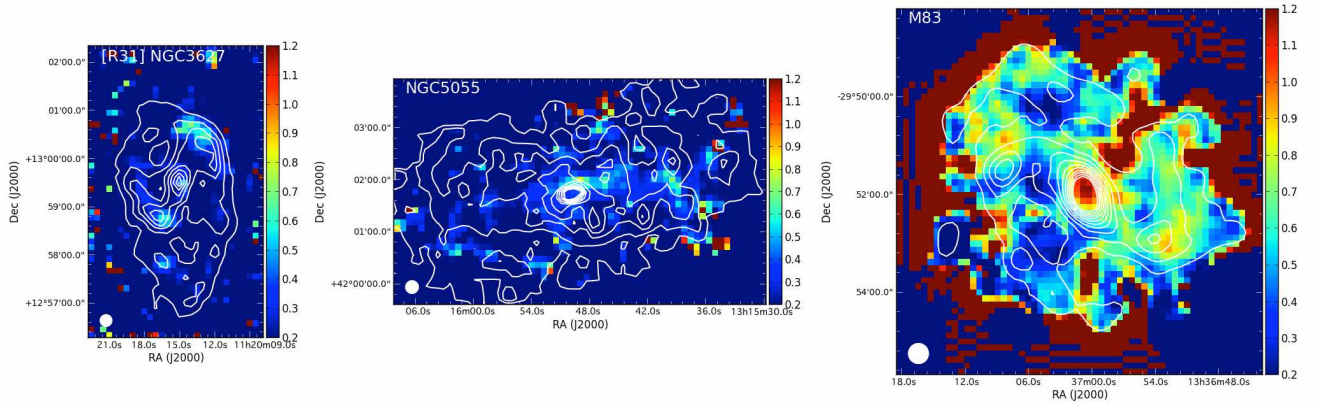


FIG. 4.— R_{31} maps of the sample galaxies. Intensity scales are set to be identical among the galaxies. The spatial resolutions are shown on the bottom-left corner of each plot. The pixel sizes are set to 7.3 arcsec for NGC 3627, 7.0 arcsec for NGC 5055 and 7.5 arcsec for M 83. As in Figure 3, Σ_{gas} distribution is shown as white contours as a reference.

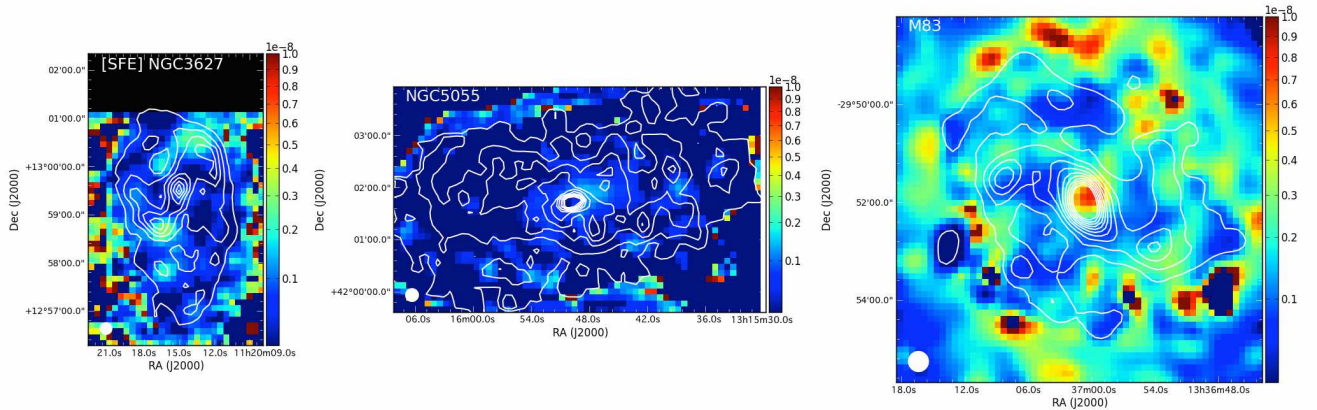


FIG. 5.— SFE (yr^{-1}) maps of the sample galaxies. Intensity scales are set to be identical among the galaxies. The unit for the color bar is yr^{-1} . The spatial resolutions are shown on the bottom-left corner of each plot. The pixel sizes are set to 7.3 arcsec for NGC 3627, 7.0 arcsec for NGC 5055 and 7.5 arcsec for M 83. As in Figure 3, Σ_{gas} distribution is shown as white contours as a reference.

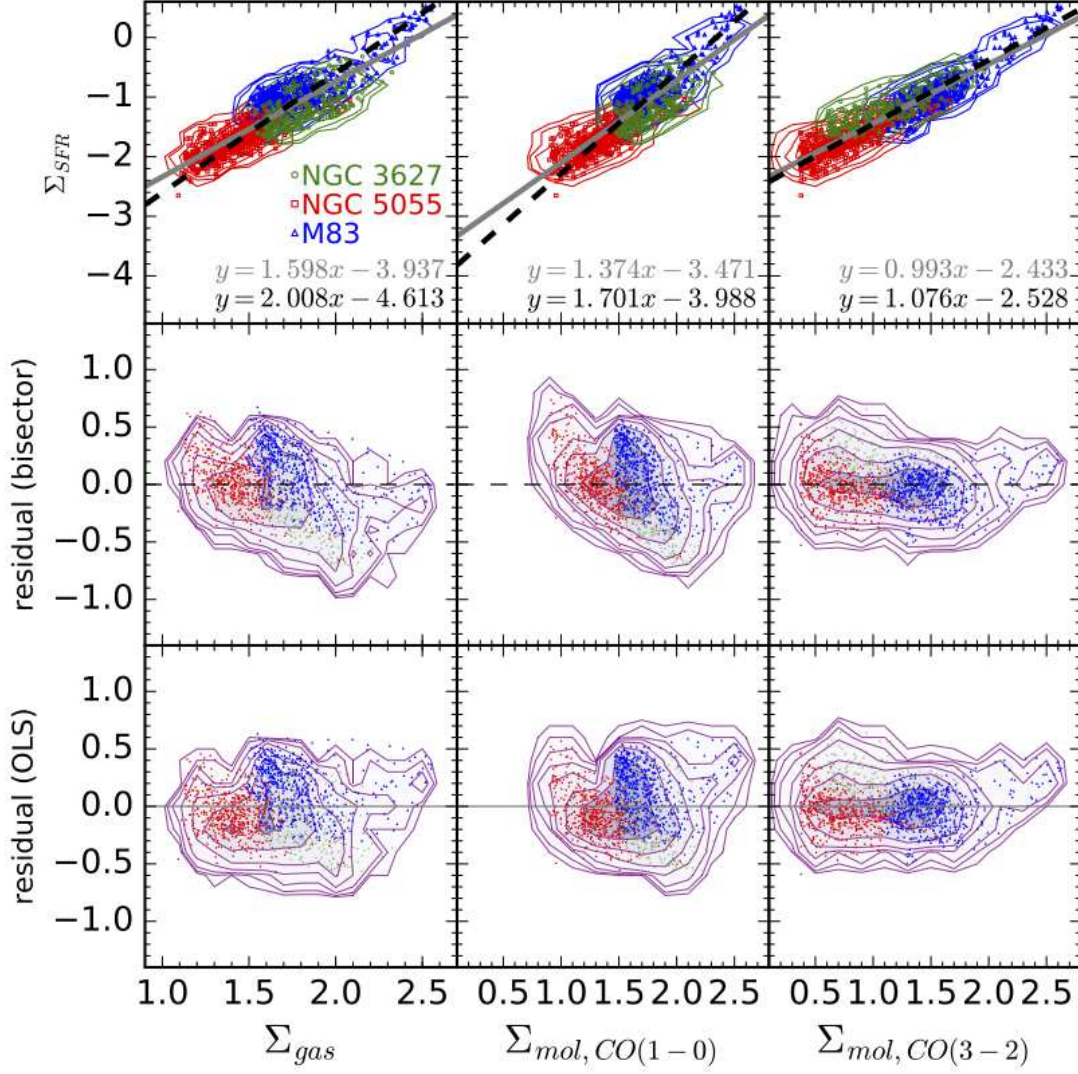


FIG. 6.— [1st row] KS relation (left), CO(1-0)-based (center) and CO(3-2)-based (right) molecular KS relation plots with the observational data of NGC 3627 (green circle and contour), NGC 5055 (red square and contour) and M 83 (blue triangle and contour). Fitting results are shown at the bottom right corner of each panel, OLS($\Sigma_{\text{SFR}}|\Sigma_{\text{gas}}$) in grey (solid) and bisector in black (dash). [2nd & 3rd rows] Residual plots of bisector fitting (2nd row) and OLS($\Sigma_{\text{SFR}}|\Sigma_{\text{gas}}$) fitting (3rd row) for each KS relation. Contours show the density of all the data points for three galaxies. $\Sigma_{\text{mol, CO(3-2)}}$ is inferred from CO(3-2) by assuming the same X_{CO} for CO(1-0) without CO(3-2)-to-CO(1-0) conversion. The qualitative trend in KS relation is similar to molecular KS relation since the galactic areas we studied are molecular-dominant region ($\text{H}_2/\text{HI} > 1$). The slope of CO(3-2)-based molecular KS relation is linear whereas the CO(1-0)-based one is super-linear, suggesting the difficulty in deriving molecular KS relation from CO(3-2) with a fixed CO(3-2)-to-CO(1-0) conversion factor.

TABLE 2
SLOPES AND NORMALIZATIONS FOR EACH R_{31} SUBSAMPLE

R_{31}	OLS($\Sigma_{\text{SFR}} \Sigma_{\text{gas}}$)		Bisector	
	Slope	Normalization	Slope	Normalization
< 0.2	1.32 ± 0.05	$-(3.71 \pm 0.08)$	1.62 ± 0.06	$-(4.19 \pm 0.09)$
0.2 – 0.4	1.27 ± 0.03	$-(3.53 \pm 0.04)$	1.47 ± 0.03	$-(3.84 \pm 0.05)$
0.4 – 0.6	1.37 ± 0.04	$-(3.48 \pm 0.07)$	1.65 ± 0.05	$-(3.94 \pm 0.08)$
0.6 – 0.8	1.11 ± 0.05	$-(2.88 \pm 0.10)$	1.53 ± 0.07	$-(3.61 \pm 0.12)$
0.8 – 1.5	1.46 ± 0.05	$-(3.34 \pm 0.10)$	1.55 ± 0.05	$-(3.51 \pm 0.10)$
0.2 – 1.5	1.60 ± 0.03	$-(3.94 \pm 0.04)$	2.01 ± 0.03	$-(4.61 \pm 0.05)$

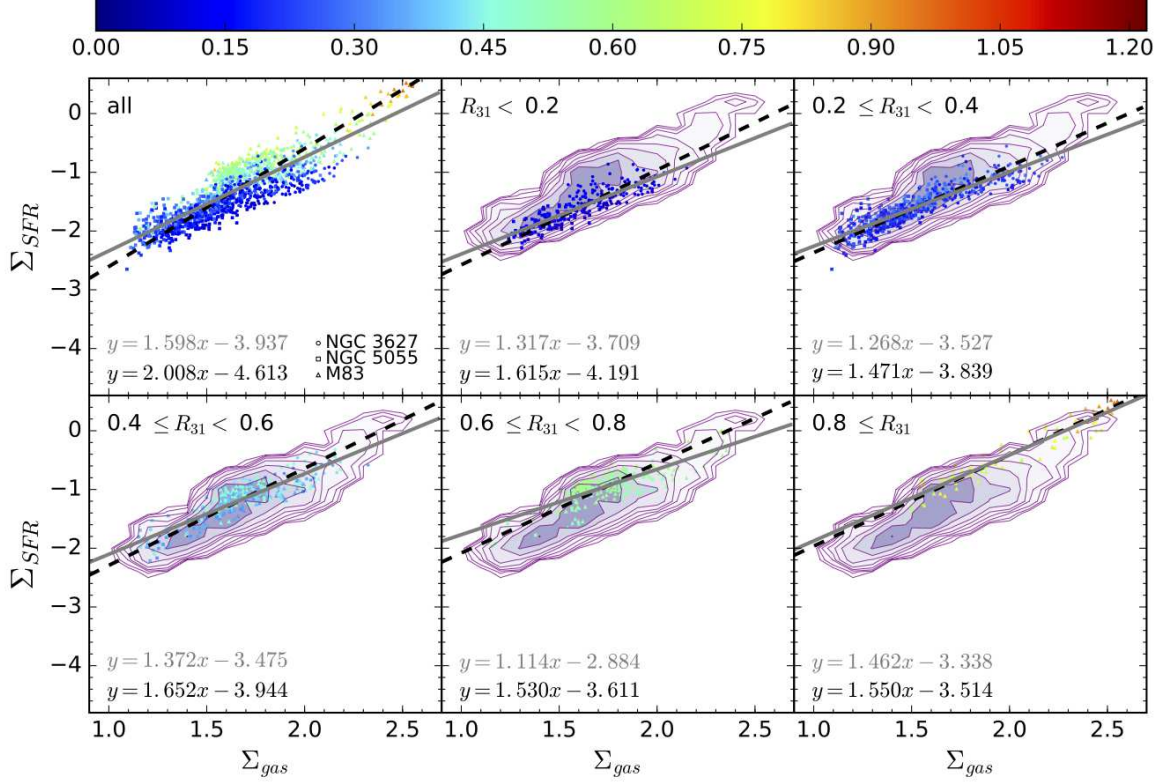


FIG. 7.— KS relation plots with the observational data of NGC 3627 (triangle), NGC 5055 (circle) and M 83 (square) color-coded for ranges of the integrated intensity ratio $R_{31} = \frac{\text{CO}(3-2)}{\text{CO}(1-0)}$. The contours show the density plots for whole sample as a reference. Resultant KS-relation slopes are shown at the bottom right corner of each panel, OLS($\Sigma_{\text{SFR}}|\Sigma_{\text{gas}}$) in grey and bisector in black. The slopes for each subcategory with a fixed range of R_{31} are shallower than the one for the whole sample. The normalizations for high R_{31} subsamples tend to be high.

blue, green, and red symbols indicate M 83, NGC 3627, and NGC 5055, respectively. This correlation has been already reported for nuclei of 60 nearby IR bright galaxies (Yao et al. 2003) and for M 83 data (Muraoka et al. 2007). We confirm that the correlation is seen even when adding the data of NGC 3627 and NGC 5055 to that of M 83.

Figure 9 shows the relationship between SFE and Σ_{gas} . For each galaxy, there is no clear dependence of SFE on Σ_{gas} , except for M 83: M 83 has outliers with high Σ_{gas} and SFE. If the data for all the galaxies are combined, a weak Σ_{gas} dependence of SFE is observed, even when excluding the outlier data points with high Σ_{gas} and SFE values from M 83. This explains the super-linear KS relation of our samples; if there is no Σ_{gas} dependence of SFE among the samples, the resulting KS-relation slope is expected to be linear.

There is a similar trend in the R_{31} - Σ_{gas} relationship in Figure 10. This agrees with our expectations, since there exists a correlation between SFE and R_{31} (Figure 8). Therefore, the distribution in the R_{31} - Σ_{gas} plane of the sample used to investigate the KS relation affects the slope of the resulting KS relation. We summarize the relation between the location of sample galaxies in the Σ_{gas} - R_{31} plane and the resulting KS relation in Figure 11. If a bimodal distribution exists along the R_{31} direction in Σ_{gas} - R_{31} space, one obtains a KS relation with two sequences. M 83 shows a faint bimodal distribution in Figure 7: one from the majority (disk region in Fig-

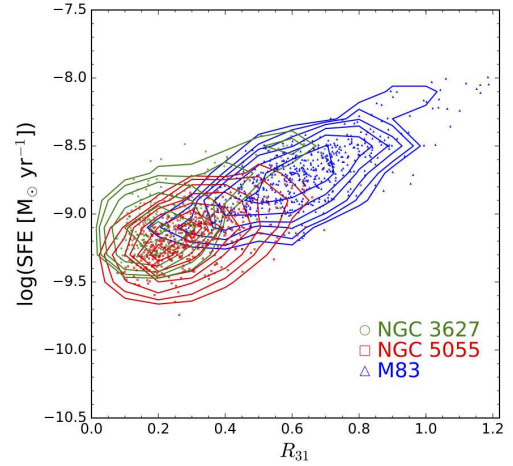


FIG. 8.— R_{31} and SFE of NGC 3627 (green circle and contour), NGC 5055 (red square and contour) and M 83 (blue triangle and contour). R_{31} is correlated with SFE over nearly 2 dex.

ure 4) and the other from the outliers (nuclear starburst region) in Σ_{gas} - R_{31} space. In Figure 10, we also notice that our three sample galaxies distribute differently in the R_{31} - Σ_{gas} plane, even though they share similar stellar mass and SFR, -i.e., they are the same galaxy populations as a first-order approximation. More specifically,

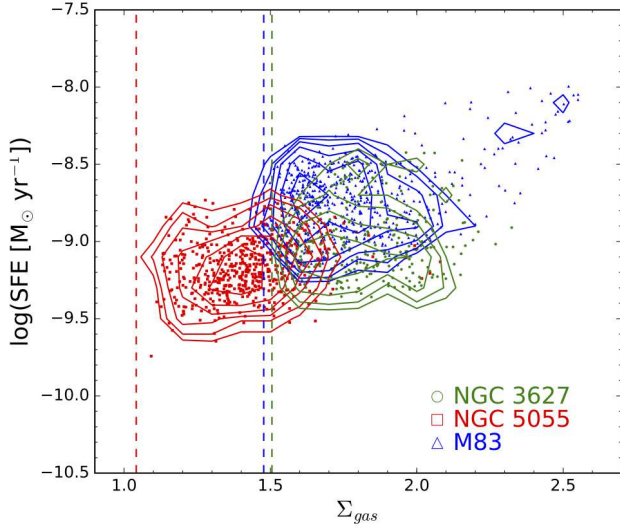


FIG. 9.— Σ_{gas} and SFE. Symbols are the same as Figure 8. Blue/red/green dashed lines represent the sensitivities of Σ_{gas} measurements for M 83 ($30 \text{ M}_{\odot} \text{ pc}^{-2}$)/ NGC 5055 (11)/NGC 3627 (32). The boundaries of lower Σ_{gas} for each galaxy are determined by the sensitivities. The distributions are different from galaxy to galaxy. The weak but existing positive dependence of SFE on Σ_{gas} generates a super-linear KS relation.

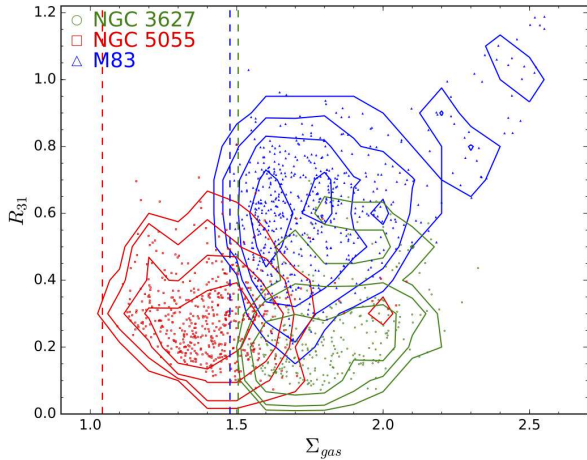


FIG. 10.— Σ_{gas} and R_{31} . Symbols are the same as Figure 8. Blue/red/green dashed lines represent the sensitivities of Σ_{gas} measurements for M 83 ($30 \text{ M}_{\odot} \text{ pc}^{-2}$)/ NGC 5055 (11)/NGC 3627 (32). The trend is almost identical with Figure 9, since R_{31} is correlated with SFE (see Figure 8).

M 83 has higher R_{31} ratio than NGC 3627 while they share similar Σ_{gas} , and on the other hand, NGC 3627 has a higher Σ_{gas} value than NGC 5055 while they share similar R_{31} .

4. HIERARCHICAL KS RELATION AND RATE-LIMITING STEP FOR STAR FORMATION

In the previous section, we showed that the R_{31} - Σ_{gas} relation is different from galaxy to galaxy and its variety can impose the variety on the resultant KS relation. In this section, we first define a “hierarchical KS relation”,

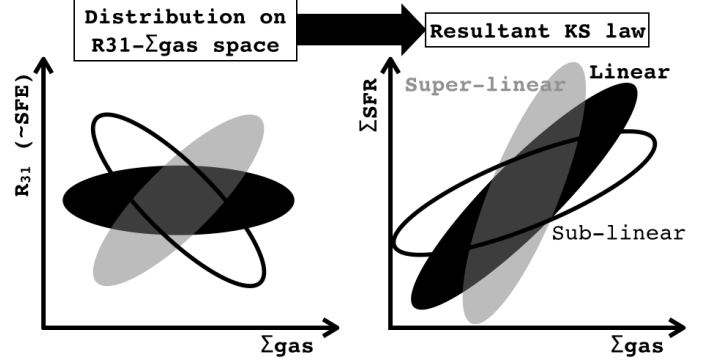


FIG. 11.— Relationship between the distribution of samples in the R_{31} - Σ_{gas} plane (left) and the resulting KS relation (right). The positive/no/negative correlations in R_{31} - Σ_{gas} result in super-linear/linear/sub-linear KS-relation slopes.

and consider our result in its context. Then, we discuss a rate-limiting hierarchical ISM step that induces a variety in the KS relation of disk galaxies and the relationship with the galactic structures.

4.1. Hierarchical KS relation

There exists a hierarchy in the ISM within a galaxy (Bergin & Tafalla 2007): cores that make up the material of stars in which the mass of the core correlates linearly with SFR (example tracer: HCN, mass of $0.5 - 5 \text{ M}_{\odot}$, size of $0.03 - 0.2 \text{ pc}$, and the mean density of $10^4 - 10^5 \text{ cm}^{-3}$), clumps ($^{13}\text{CO}(1-0)$, $50 - 500 \text{ M}_{\odot}$, $0.3 - 3 \text{ pc}$, and $10^3 - 10^4 \text{ cm}^{-3}$), molecular clouds ($^{13}\text{CO}(1-0)$ and $^{12}\text{CO}(1-0)$, $10^3 - 10^4 \text{ M}_{\odot}$, $2 - 15 \text{ pc}$, $50 - 500 \text{ cm}^{-3}$), and diffuse atomic gas. In addition, some studies also suggested the existence of substantial amounts of volume-filling molecules or diffuse small clouds traced by CO(1-0) in Galactic sources (Polk et al. 1988; Knapp & Bowers 1988; Carpenter et al. 1995; Heyer et al. 1996; Hily-Blant & Falgarone 2007; Goldsmith et al. 2008; Roman-Duval et al. 2016) as well as extragalactic sources (Young & Sanders 1986; Wilson & Walker 1994; Rosolowsky et al. 2007; Pety et al. 2013; Caldú-Primo et al. 2013; Rahman et al. 2011; Shetty et al. 2014b,a; Morokuma-Matsui et al. 2015). Considering that the transitions between diffuse gas and self-gravitating gas, and between atomic gas and molecular gas depend differently on the ISM properties, the existence of non-self gravitating molecular gas traced by CO is not surprising (e.g., Elmegreen 1993).

The KS relation connects the amount of total gas and SFR of a galaxy or a certain region of galaxies. Considering the hierarchy in the ISM, there are mainly four steps for star formation from gas: conversions from atomic gas to molecular gas, from molecular gas to molecular clouds, from molecular clouds to dense cores⁴, and from dense

⁴ Here, we do not distinguish clumps from clouds since they are relatively similar compared to cores in terms of size and mass. Nowadays, the filaments found in molecular clouds are considered to correspond to clumps. The *Herschel* satellite revealed the ubiquity of filamentary structures (e.g., André et al. 2010) and it is shown that both cores for massive and low mass stars are formed in the $\sim 0.1 \text{ pc}$ -wide filaments (André et al. 2016). The core mass fraction over filament and filament mass fraction over molecular clouds should be measured in future.

cores to stars. We define the hierarchical KS relation as,

$$\Sigma_{\text{SFR}} \propto f_{\text{core}} f_{\text{SF,cloud}} f_{\text{cloud}} f_{\text{mol}} \Sigma_{\text{gas}}, \quad (2)$$

where $f_{\text{core}} = \Sigma_{\text{core}}/\Sigma_{\text{SF,cloud}}$ (a ratio of surface densities of dense core, Σ_{core} , within a cloud and its parent star-forming cloud, $\Sigma_{\text{SF,cloud}}$, conversion efficiency from star-forming cloud to the dense core), $f_{\text{SF,cloud}} = \Sigma_{\text{SF,cloud}}/\Sigma_{\text{cloud}}$ (a ratio of surface densities of the star-forming cloud and all the molecular clouds, Σ_{cloud}), $f_{\text{cloud}} = \Sigma_{\text{cloud}}/\Sigma_{\text{mol}}$ (a ratio of surface densities of molecular clouds and molecular gas, Σ_{mol}), and $f_{\text{mol}} = \Sigma_{\text{mol}}/\Sigma_{\text{gas}}$ (the ratio of surface densities of molecular gas and total gas, Σ_{gas}). The surface areas used to calculate surface densities are defined by the spatial resolution of the observations.

Equation (2) is derived by assuming a linear relation of $\Sigma_{\text{SFR}} \propto \Sigma_{\text{core}}$ claimed in the previous studies (e.g., Solomon et al. 1992; Gao & Solomon 2004a,b; Wu et al. 2005)⁵. No clear dependence of f_{core} on $\Sigma_{\text{SF,cloud}}$ (\sim CO(3-2) surface density) was reported based on low-mass star forming regions of our Galaxy, which supports a constant f_{core} (Battisti & Heyer 2014, but see also Meidt 2016). In addition, the linear relation of SFR-CO(3-2) seen in this study (Figure 6, right) as well as previous studies (Narayanan et al. 2005; Komugi et al. 2007; Bayet et al. 2009; Iono et al. 2009; Mao et al. 2010; Greve et al. 2014; Muraoka et al. 2016) suggests $\Sigma_{\text{SFR}} \propto \Sigma_{\text{SF,cloud}}$, accordingly a constant f_{core} . It is important to investigate the conversion efficiency of each step and controlling factors for each efficiency, and then specify the rate-limiting step of star formation.

4.2. ISM hierarchical step inducing variety in the KS relation

We showed that SFE is correlated with R_{31} in Figure 8, suggesting that R_{31} is one of the keys to determining star formation. If we assume that CO(1-0) and CO(3-2) emissions respectively trace total molecular gas and star-forming molecular clouds⁶, the R_{31} value is a measure of a ratio of $\Sigma_{\text{SF,cloud}}/\Sigma_{\text{mol}}$, which corresponds to a product of $f_{\text{SF,cloud}}$ and f_{cloud} in Equation (2). At this point, it is not clear which ISM hierarchical step, formations of molecular cloud (f_{cloud}) or star-forming molecular cloud ($f_{\text{SF,cloud}}$), induces the R_{31} variety since $\Sigma_{\text{SF,cloud}}/\Sigma_{\text{mol}}$ is a product of f_{cloud} and $f_{\text{SF,cloud}}$.

We summarize the previous studies related to f_{cloud} and $f_{\text{SF,cloud}}$ of galaxies in this section. Note that there is no previous study on f_{cloud} and $f_{\text{SF,cloud}}$ exactly in consideration of Equation (2).

f_{cloud} values for each galaxy were reported to be ~ 0.5 , however there is a variety as a function of galactic structure. Wilson & Walker (1994) reported $f_{\text{cloud}} \sim 0.4-0.7$ for M 33 based on a comparison of $^{12}\text{CO}(1-0)$ and

$^{13}\text{CO}(1-0)$ emission. For M 33, Rosolowsky et al. (2007) found a radial gradient of f_{cloud} in high-spatial resolution CO(1-0) maps: 0.6 at the galactic center and 0.2 at 4 kpc from the center. Pety et al. (2013) concluded that a half of the $^{12}\text{CO}(1-0)$ flux of M 51 is from diffuse molecular gas suggested as a missing flux of the interferometric observations. Assuming the same CO-to-H₂ conversion factor for molecular clouds and diffuse molecular gas, their study suggests f_{cloud} is expected to be ~ 0.5 . For one of the early-type galaxies, NGC 4526, f_{cloud} is reported to be ~ 0.5 (Utomo et al. 2015). In addition, using spatially resolved $^{12}\text{CO}(1-0)$ and $^{13}\text{CO}(1-0)$ data, higher f_{cloud} in the spiral arms than the inter-arm region is suggested in the Milky Way (Sawada et al. 2012b,a) and NGC 3627 (Morokuma-Matsui et al. 2015).

Although there is no direct measurements of $f_{\text{SF,cloud}}$, the number fraction of star-forming molecular clouds over all the molecular clouds ($R_{\text{SF,cloud}} = N_{\text{SF,cloud}}/N_{\text{cloud}}$, where $N_{\text{SF,cloud}}$ and N_{cloud} are the numbers of star-forming and total clouds, respectively) has been investigated. Kawamura et al. (2009) classified molecular clouds in the Large Magellanic Cloud (LMC) based on the contiguity of clouds with H II regions and stellar clusters. They found that $R_{\text{SF,cloud}}$ is ~ 0.7 . A similar value was also reported in M 33 (Miura et al. 2012)⁷.

To convert $R_{\text{SF,cloud}}$ to $f_{\text{SF,cloud}}$, we must take into account the molecular cloud mass dependence of $R_{\text{SF,cloud}}$ and the mass spectrum of molecular clouds, since there is a variety in the masses of molecular clouds. Engargiola et al. (2003) showed that massive molecular clouds tend to have higher $R_{\text{SF,cloud}}$ values than low-mass molecular clouds. For a variety in mass spectrum of molecular clouds of Local Group galaxies, Rosolowsky (2005) reported a steeper mass function (i.e., smaller contribution of large molecular clouds) for the outer disk of the Milky Way and M 33 compared to the inner disk of the Milky Way (comparison of the mass spectra among Local Group galaxies is found in Figure 9 of Blitz et al. 2007). Recently, a steeper mass spectrum was reported in early-type galaxy, NGC 4526 (Utomo et al. 2015). In addition, it is shown that massive molecular clouds are likely to be found at the spiral arms in M 51 (Koda et al. 2009; Colombo et al. 2014). These studies suggest that $f_{\text{SF,cloud}}$ has a variety among galaxies, although the variation in the mass distributions has not been fully understood.

4.3. What determines $R_{31} \sim f_{\text{SF,cloud}} \times f_{\text{cloud}}$ within a galaxy?

In this section, we discuss what determines f_{cloud} and/or $f_{\text{SF,cloud}}$ in galaxies. A weak positive correlation seen in Figure 10 suggests that high Σ_{gas} is one of the necessary conditions for high f_{cloud} and/or $f_{\text{SF,cloud}}$ ⁸.

⁵ A sub-linear relation between Σ_{SFR} and Σ_{core} has been reported if limiting the sample to normal disk galaxies (Usero et al. 2015; Chen et al. 2015; Bigiel et al. 2016).

⁶ The f_{mol} variety can impose the variety in the KS relation. f_{mol} is shown to be higher for more massive galaxies than lower mass galaxies (e.g., Bothwell et al. 2014), and higher at the smaller galactic radius than larger radius (e.g., Schrubba et al. 2011; Tanaka et al. 2014). Though in this study we focus on the relatively massive galaxies and their optical disks where f_{mol} is evenly high, f_{mol} may be a main contributor of the diversity of the KS relation in the atomic gas dominated environments, such as low mass galaxies and galaxy outskirts.

⁷ Minamidani et al. (2008) found that the R_{31} is higher for molecular clouds with H II region and stellar clusters than the molecular clouds without them in LMC, and the same trend is confirmed in M 33 (Miura et al. 2012). This supports the idea that CO(3-2) traces the star-forming molecular clouds.

⁸ If X_{CO} is a function of R_{31} , the weak positive correlation observed in $R_{31}-\Sigma_{\text{gas}}$ plot become steeper. It is because the high R_{31} gas is expected to have relatively high gas temperature (e.g., Minamidani et al. 2008), accordingly smaller X_{CO} . This would work in the left direction in $R_{31}-\Sigma_{\text{gas}}$ plot for high- Σ_{gas} and R_{31} data points. Therefore, this may increase the KS-relation slope but

The major differences between the high- Σ_{gas} galaxies (NGC 3627 and M 83) and low- Σ_{gas} galaxy (NGC 5055) in our sample is the existence of galactic-scale structures such as spiral arms and bars: NGC 3627 and M 83 are classified as barred-spiral galaxies with grand design spirals whereas NGC 5055 is a spiral galaxy with flocculent spiral arms (Elmegreen & Elmegreen 1987). High gas density at the spiral arm, bar and central regions is seen in Figure 3 and reported in many observational studies (e.g., Helfer et al. 2003; Kuno et al. 2007).

Theoretical studies predict gas compression at spiral arms, i.e., the “galactic shock” in density wave theory (Fujimoto 1968; Roberts 1969; Shu et al. 1973) and a “large-scale colliding flow” in the dynamic spiral theory (Dobbs & Bonnell 2008; Wada et al. 2011; Baba et al. 2017). A high gas density at the bar-end and leading-edge of the bar region is expected from the crowded orbits there (Wada 1994). In addition, the bar structures are predicted to play a role in removing angular momentum, thus inducing gas inflow to the galactic center (e.g., Wada & Habe 1992). Observations confirmed a higher gas density at the central regions of barred spiral galaxies compared to non-barred galaxies (Sakamoto et al. 1999; Kuno et al. 2007).

We can see that the downstream side of bar-end region have high R_{31} and SFE in both NGC 3627 and M 83 in Figures 4 and 5. The offset between molecular gas and star formation at bar regions has been reported in Sheth et al. (2002) based on interferometric observations. They showed that H α emission is offset towards the downstream side of CO(1-0) not only at the bar-end but also within the bar, and the largest offsets are found in the strongest bars. Kenney & Lord (1991) suggested that the offset star-forming regions in the downstream side of the bar-end in M 83 were presumably triggered as the gas passes through the transition regions of bar and spiral arms. In addition, the enhancement of R_{31} or SFE at the offset regions may be related to the smaller velocity dispersion of molecular gas there than bar-end region of NGC 3627 reported in Morokuma-Matsui et al. (2015). The reduced random motion induces star formation.

Combined with the previous studies showing a high f_{cloud} and abundance of massive molecular clouds in spiral arms, our results suggest that galactic structures (dynamics) affect Σ_{gas} distribution, consequently $R_{31} \sim f_{\text{cloud}} \times f_{\text{SF,cloud}}$, and then star formation in galaxies. It is theoretically predicted that gas compression increases not only Σ_{gas} but also f_{cloud} (Inoue & Inutsuka 2008, 2009), and possibly $f_{\text{SF,cloud}}$. However, high Σ_{gas} is not a sufficient condition for high f_{cloud} and/or $f_{\text{SF,cloud}}$. In Figure 10, we can see that M 83 has higher R_{31} ratio than NGC 3627 while they share similar Σ_{gas} . To explore the hierarchical KS relation in more depth, we must increase the number of samples and spatial resolution

and directly measure the f_{cloud} and $f_{\text{SF,cloud}}$ using the newest-generation instruments such as the Atacama Large Millimeter /submillimeter Array (ALMA), and the Northern Extended Millimeter Array (NOEMA).

The R_{31} dependence of the KS-relation slopes was investigated. We combined the literature maps of H I, CO(1-0), CO(3-2), H α , 24 μm of three nearby spiral galaxies – NGC 3627, NGC 5055, and M 83 – and estimated their Σ_{gas} and Σ_{SFR} . The main results are as follows.

- The slopes for the KS relations of the samples subdivided by R_{31} are shallower than that for all of the datasets combined. The normalizations for high- R_{31} samples tend to be higher than those for the low- R_{31} counterparts.
- The KS-relation slopes change according to the distribution in R_{31} - Σ_{gas} space of the plotted samples; no Σ_{gas} dependence of R_{31} results in a linear slope of the KS-relation whereas a positive correlation between Σ_{gas} and R_{31} results in a super-linear slope of the KS-relation.
- The R_{31} - Σ_{gas} distribution is different from galaxy to galaxy as well as within a galaxy. High Σ_{gas} and R_{31} are found at the central and the bar-end regions suggesting that galactic structures (dynamics) play a role in determining the galactic KS relation.

We also discuss the rate-limiting ISM hierarchical step of star formation by introducing the concept of a hierarchical KS relation. Assuming a linear relationship between core mass and SFR, the KS relation can be re-written as Equation (2). Since R_{31} is a measure of star-forming cloud fraction among total clouds, – i.e., a product of $f_{\text{SF,cloud}}$ and f_{cloud} , our result suggests that $f_{\text{SF,cloud}}$ and/or f_{cloud} is the rate-limiting ISM hierarchy which imposes a diversity on the resultant KS relation. It is still unclear which ISM hierarchy, $f_{\text{SF,cloud}}$ or f_{cloud} , is the main contributor imposing large variation in the KS relation both within a galaxy and among galaxies in relatively high- Σ_{gas} regimes. High spatial resolution and high sensitivity observations in CO(1-0) to measure f_{cloud} and $f_{\text{SF,cloud}}$ are required to reveal the origin of the KS-relation diversity.

We are grateful to anonymous referee, Dr. Junichi Baba, Dr. Tomoki Morokuma, Dr. Shinya Komugi, Dr. Robert C. Kennicutt, Dr. Tsutomu Takeuchi, Dr. Kouichiro Nakanishi, Dr. Fumi Egusa and Dr. Nario Kuno for enlightening comments and suggestions. We thank Dr. Eric Feigelson for his constructive comments on the statistical aspects. KM thanks Dr. Ross Burns for English language editing.

APPENDIX

DIFFUSE EMISSION SUBTRACTION FOR SFR ESTIMATION

In section 2.2, Σ_{SFR} is estimated from H α and 24 μm maps of the galaxies under an assumption that all the H α emitting gas is ionized by the localized star formation in the same region. However, the kpc-scale extra-planar ionized

5. CONCLUSIONS

cannot make the super-linear KS-relation linear or sub-linear.

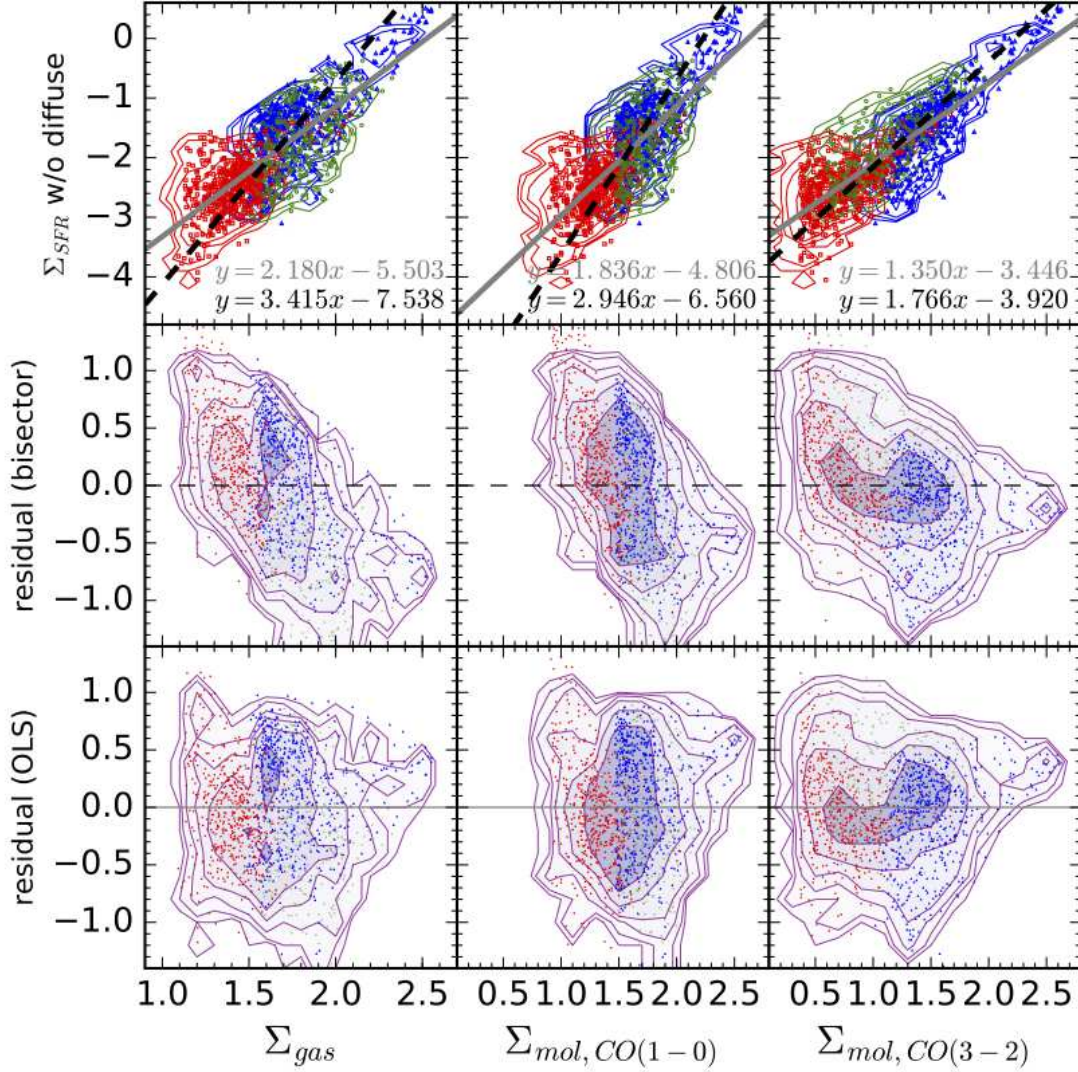


FIG. 12.— Same figures as Figure 6 but with diffuse emission subtracted. [1st row] KS relation (left), CO(1-0)-based (center) and CO(3-2)-based (right) molecular KS relation plots with the observational data of NGC 3627 (green circle and contour), NGC 5055 (red square and contour) and M 83 (blue triangle and contour). Fitting results are shown at the bottom right corner of each panel, OLS($\Sigma_{\text{SFR}}|\Sigma_{\text{gas}}$) in grey (solid) and bisector in black (dash). [2nd & 3rd rows] Residual plots of the bisector fitting (2nd row) and the OLS($\Sigma_{\text{SFR}}|\Sigma_{\text{gas}}$) fitting (3rd row) for each KS relation. Contours show the density of all the data points for the three galaxies. The slopes are steeper and the scatters are larger than those seen in Figure 6.

TABLE 3
SLOPES AND NORMALIZATIONS FOR EACH R_{31} SUBSAMPLE (W/O DIFFUSE SFR)

R_{31}	OLS($\Sigma_{\text{SFR}} \Sigma_{\text{gas}}$)		Bisector	
	Slope	Normalization	Slope	Normalization
< 0.2	1.62 ± 0.13	$-(4.96 \pm 0.21)$	3.57 ± 0.25	$-(8.12 \pm 0.41)$
0.2 – 0.4	1.70 ± 0.07	$-(4.88 \pm 0.11)$	2.81 ± 0.11	$-(6.59 \pm 0.16)$
0.4 – 0.6	1.90 ± 0.10	$-(4.92 \pm 0.17)$	3.31 ± 0.17	$-(7.28 \pm 0.28)$
0.6 – 0.8	1.72 ± 0.12	$-(4.42 \pm 0.21)$	3.54 ± 0.23	$-(7.62 \pm 0.41)$
0.8 – 1.5	2.07 ± 0.09	$-(4.83 \pm 0.18)$	2.30 ± 0.09	$-(5.28 \pm 0.19)$
0.2 – 1.5	2.18 ± 0.05	$-(5.50 \pm 0.08)$	3.41 ± 0.07	$-(7.54 \pm 0.12)$

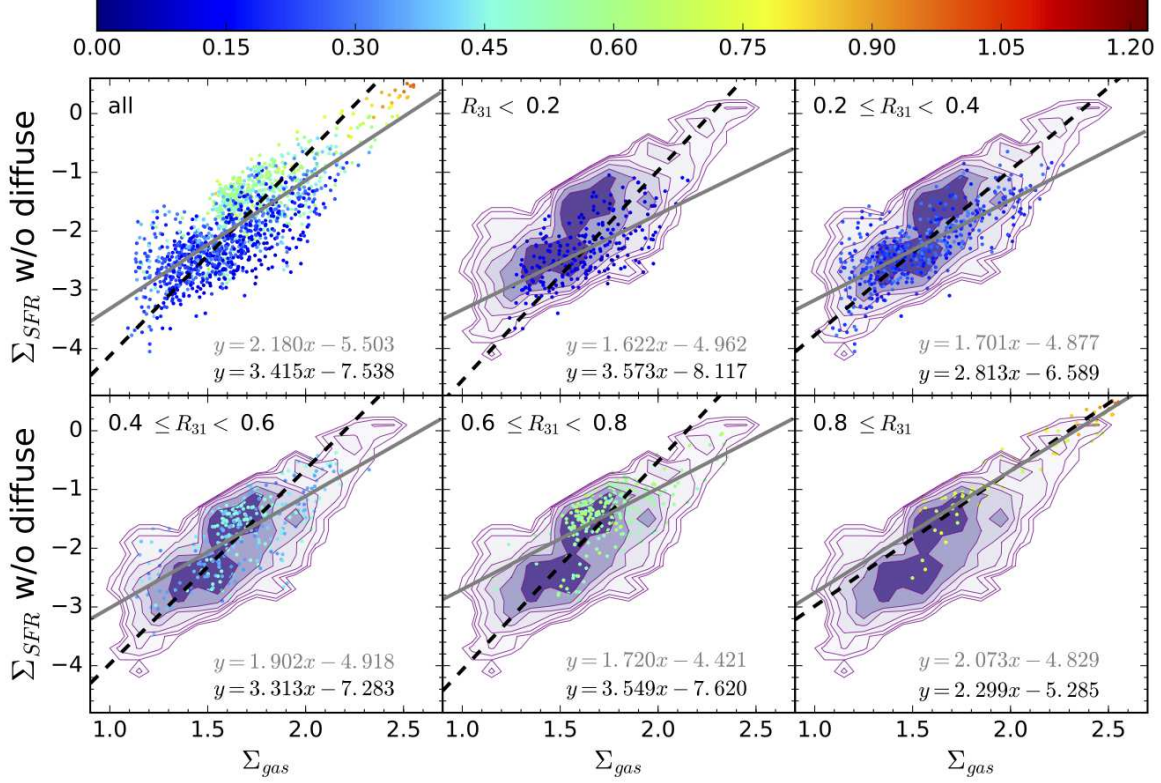


FIG. 13.— Same figures as Figure 7 but with diffuse emission subtracted data. KS relation plots with the observational data of NGC 3627 (triangle), NGC 5055 (circle) and M 83 (square) color-coded for ranges of the integrated intensity ratio $R_{31} = \frac{\text{CO}(3-2)}{\text{CO}(1-0)}$. The contours show the density plots for whole sample as a reference. Resultant KS-relation slopes are shown at the bottom right corner of each panel, OLS($\Sigma_{\text{SFR}}|\Sigma_{\text{gas}}$) in grey and bisector in black. The trends are similar to the ones seen in Figure 7 where the slopes for each subcategory with a fixed range of R_{31} tend to be shallower than the one for the whole sample and the normalizations for high R_{31} subsamples tend to be high.

TABLE 4
AIC OF THE POLYNOMIAL FITTING MODEL FOR KS RELATION

	1st	2nd	3rd	4th	5th	6th
w/ diffuse	4.478	4.095	-42.12	-105.5	-138.2	<u>-155.0</u>
w/o diffuse	1734	1724	1721	1705	1697	<u>1684</u>

NOTE. — The minima are shown with underline.

gas has been observed especially in edge-on galaxies, e.g., M 82 (e.g., Lynds & Sandage 1963), indicating that ionizing radiation can reach farther than the sizes of an H II region of $\sim 0.1 - 10$ pc in the Milky Way (e.g., Kennicutt 1984; Garay & Lizano 1999). The theoretical studies predict a larger escape fraction of ionizing radiation if the ISM is not smooth but structured (Haffner et al. 2009, references therein). Therefore, the H α emitting gas is not necessarily ionized by the localized star formation in the same region.

To distinguish a H II region from diffuse ionized gas and estimate Σ_{SFR} accurately, differences in spectroscopic property (Madsen et al. 2006; Blanc et al. 2009) and spatial distribution (e.g., Thilker et al. 2000; Liu et al. 2011) have been used. In this study, we applied *HIIphot*, an IDL software developed by Thilker et al. (2000), to H α and 24 μm data to distinguish compact component from diffuse emission, following the procedures in Liu et al. (2011).

Figure 12 is the same as Figure 6 but using Σ_{SFR} without diffuse emission. As previous studies claimed (Liu et al. 2011; Momose et al. 2013), the resultant slopes become steeper since the contribution from diffuse emission is larger at lower Σ_{SFR} regime. The increase in the scatter after subtraction of diffuse emission is also consistent with Liu et al. (2011).

Again, Figure 13 is the same as Figure 7 but using Σ_{SFR} without diffuse emission. In Figure 13 and Table 3, we confirmed the same trends seen in Figure 7 and Table 2 where the slopes for the KS relations of the samples subdivided by R_{31} are shallower than that for all the datasets combined and the normalizations for high- R_{31} data tend to be higher than those for the low- R_{31} counterparts. Therefore, the contribution from diffuse ionized gas changes the slopes of the KS-relation but does not change the trends we obtained using Σ_{SFR} with diffuse H α and 24 μm emission.

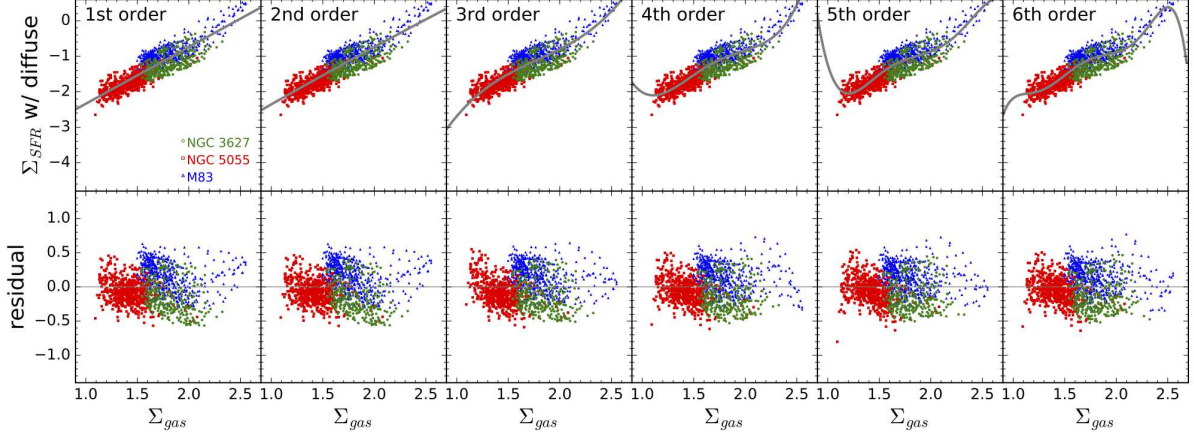


FIG. 14.— Result of the polynomial fitting (grey solid line) to the KS relation with the observational data of NGC 3627 (green triangle), NGC 5055 (red circle) and M 83 (blue square). Diffuse emission is not subtracted from Σ_{SFR} . The residual plots are also presented in the bottom row. The AIC for each fitting is shown in Table 4.

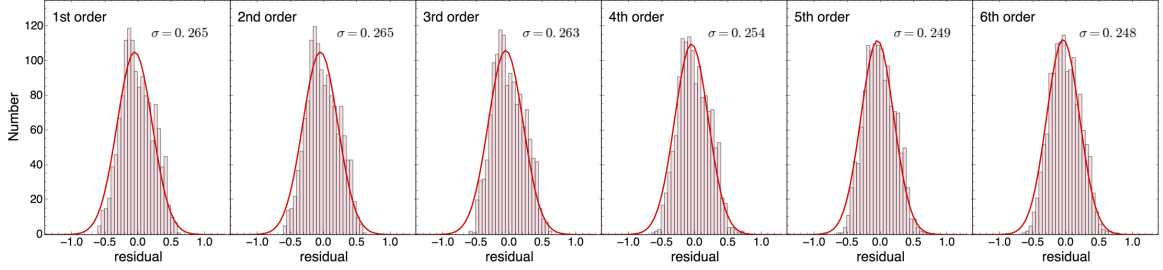


FIG. 15.— Residual distribution of Figure 14. The red solid lines show the fitting results with Gaussian whose σ is shown at upper right corner of each plot.

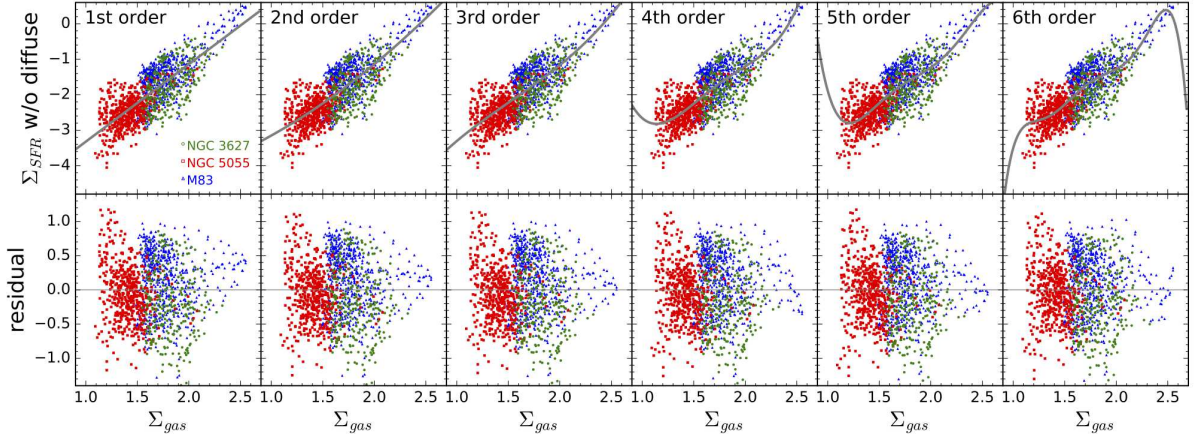


FIG. 16.— Same as Figure 14 but using Σ_{SFR} without diffuse $\text{H}\alpha$ and $24\ \mu\text{m}$ emission.

AKAIKE'S INFORMATION CRITERION FOR $\Sigma_{\text{GAS}} - \Sigma_{\text{SFR}}$ RELATION

We measure Akaike's Information Criterion (AIC, Akaike 1974) to test the validity of applying a linear fitting to the KS relation. In general, fitting with a higher order polynomial function to data performs better than that of lower degree. However, such high-order fitting is able to be *forced* to fit to the fluctuations that is not related to the true relation (“Overfitting”). The AIC can deal with trade-off between the goodness of fit of the model and the complexity of the model. The AIC is defined as

$$\text{AIC} = -2[\mathcal{L}(\hat{\theta}) - K], \quad (\text{B1})$$

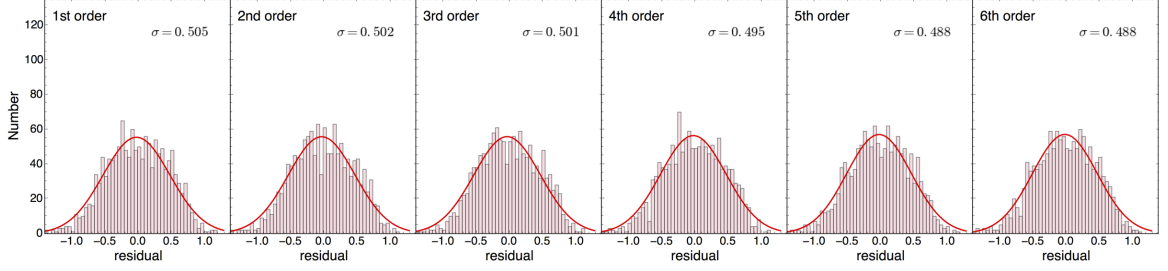


FIG. 17.— Residual distribution of Figure 16. The red solid lines show the fitting results with Gaussian whose σ is shown at upper right corner of each plot.

where \mathcal{L} is a likelihood function, $\hat{\theta}$ is a set of maximum-likelihood estimators, and K is the number of free parameters of the assumed model. The most preferred model minimizes the AIC.

Hereafter, we follow the Appendix of Takeuchi et al. (2000) to calculate the AIC. We adopted the m th order polynomial model to fit a set of n pairs of observations, $(x_1, y_1), \dots, (x_n, y_n)$ as,

$$y_i = \sum_{l=0}^m a_l x_i^l + \epsilon_i, \quad (\text{B2})$$

where we assume that ϵ_i is an independent random variable that follows the normal distribution with mean of zero and dispersion of σ^2 . In case of the normal distribution, the AIC is written as

$$\text{AIC}(m) = n(\ln 2\pi + 1) + n \ln \widehat{\sigma}^2(m) + 2(m + 2), \quad (\text{B3})$$

where

$$\widehat{\sigma}^2 = -\frac{1}{n} \sum_{i=1}^n \left(y_i - \sum_{l=0}^m \hat{a}_l x_i^l \right)^2. \quad (\text{B4})$$

We calculate the AIC for $m = 1 \sim 6$ using Equation B3.

Figures 14 and 16 show the polynomial fitting results of the KS relation with and without diffuse emission for SFR estimation, respectively. Figures 15 and 17 are the residual plots for the 1st~6th polynomial fittings in Figures 14 and 16, respectively. According to the AIC, 6th-order polynomial is the most preferable for KS relation of our three target galaxies rather than linear function (see Table 4). However, as we showed in Section 3 and previous studies, the resultant KS relation can change according to what kind of data (galaxies, regions in a galaxy and resolution) are used to plot.

REFERENCES

- Akaike, H. 1974, IEEE Transactions on Automatic Control, 19, 716
- André, P., Men'shchikov, A., Bontemps, S., et al. 2010, A&A, 518, L102
- André, P., Revéret, V., Könyves, V., et al. 2016, A&A, 592, A54
- Asplund, M., Grevesse, N., Sauval, A. J., & Scott, P. 2009, ARA&A, 47, 481
- Baba, J., Morokuma-Matsui, K., & Saitoh, T. R. 2017, MNRAS, 464, 246
- Battisti, A. J., & Heyer, M. H. 2014, ApJ, 780, 173
- Bayet, E., Gerin, M., Phillips, T. G., & Contursi, A. 2009, MNRAS, 399, 264
- Bergin, E. A., & Tafalla, M. 2007, ARA&A, 45, 339
- Bigiel, F., Leroy, A., Walter, F., et al. 2008, AJ, 136, 2846
- Bigiel, F., Leroy, A. K., Blitz, L., et al. 2015, ApJ, 815, 103
- Bigiel, F., Leroy, A. K., Jiménez-Donaire, M. J., et al. 2016, ApJ, 822, L26
- Blanc, G. A., Heiderman, A., Gebhardt, K., Evans, II, N. J., & Adams, J. 2009, ApJ, 704, 842
- Blitz, L., Fukui, Y., Kawamura, A., et al. 2007, Protostars and Planets V, 81
- Boselli, A., Fossati, M., Gavazzi, G., et al. 2015, A&A, 579, A102
- Boselli, A., Eales, S., Cortese, L., et al. 2010, PASP, 122, 261
- Bothwell, M. S., Wagg, J., Ciccone, C., et al. 2014, MNRAS, 445, 2599
- Bresolin, F., Schaerer, D., González Delgado, R. M., & Stasińska, G. 2005, A&A, 441, 981
- Caldú-Primo, A., Schruha, A., Walter, F., et al. 2013, AJ, 146, 150
- Calzetti, D., Liu, G., & Koda, J. 2012, ApJ, 752, 98
- Calzetti, D., Kennicutt, R. C., Engelbracht, C. W., et al. 2007, ApJ, 666, 870
- Carpenter, J. M., Snell, R. L., & Schloerb, F. P. 1995, ApJ, 445, 246
- Chen, H., Gao, Y., Braine, J., & Gu, Q. 2015, ApJ, 810, 140
- Colombo, D., Hughes, A., Schinnerer, E., et al. 2014, ApJ, 784, 3
- Comte, G. 1981, A&AS, 44, 441
- Cortese, L., Boissier, S., Boselli, A., et al. 2012, A&A, 544, A101
- Daddi, E., Elbaz, D., Walter, F., et al. 2010, ApJ, 714, L118
- Dale, D. A., Cohen, S. A., Johnson, L. C., et al. 2009, ApJ, 703, 517
- Dame, T. M., Hartmann, D., & Thaddeus, P. 2001, ApJ, 547, 792
- Dempsey, J. T., Thomas, H. S., & Currie, M. J. 2013, ApJS, 209, 8
- Dobbs, C. L., & Bonnell, I. A. 2008, MNRAS, 385, 1893
- Elmegreen, B. G. 1993, ApJ, 411, 170
- Elmegreen, D. M., & Elmegreen, B. G. 1987, ApJ, 314, 3
- Engargiola, G., Plambeck, R. L., Rosolowsky, E., & Blitz, L. 2003, ApJS, 149, 343
- Fujimoto, M. 1968, in IAU Symposium, Vol. 29, Non-stable Phenomena in Galaxies, 453
- Gao, Y., & Solomon, P. M. 2004a, ApJS, 152, 63
- . 2004b, ApJ, 606, 271
- Garay, G., & Lizano, S. 1999, PASP, 111, 1049

- Goldsmith, P. F., Heyer, M., Narayanan, G., et al. 2008, *ApJ*, 680, 428
- Greve, T. R., Leonidaki, I., Xilouris, E. M., et al. 2014, *ApJ*, 794, 142
- Haffner, L. M., Dettmar, R.-J., Beckman, J. E., et al. 2009, *Reviews of Modern Physics*, 81, 969
- Helfer, T. T., Thornley, M. D., Regan, M. W., et al. 2003, *ApJS*, 145, 259
- Heyer, M. H., Carpenter, J. M., & Ladd, E. F. 1996, *ApJ*, 463, 630
- Hily-Blant, P., & Falgarone, E. 2007, *A&A*, 469, 173
- Hughes, T. M., Cortese, L., Boselli, A., Gavazzi, G., & Davies, J. I. 2013, *A&A*, 550, A115
- Inoue, T., & Inutsuka, S.-i. 2008, *ApJ*, 687, 303
- . 2009, *ApJ*, 704, 161
- Iono, D., Wilson, C. D., Yun, M. S., et al. 2009, *ApJ*, 695, 1537
- Isobe, T., Feigelson, E. D., Akritas, M. G., & Babu, G. J. 1990, *ApJ*, 364, 104
- Jarrett, T. H., Masci, F., Tsai, C. W., et al. 2013, *AJ*, 145, 6
- Kawamura, A., Mizuno, Y., Minamidani, T., et al. 2009, *ApJS*, 184, 1
- Kenney, J. D. P., & Lord, S. D. 1991, *ApJ*, 381, 118
- Kennicutt, Jr., R. C. 1984, *ApJ*, 287, 116
- . 1998, *ApJ*, 498, 541
- Kennicutt, Jr., R. C., Armus, L., Bendo, G., et al. 2003, *PASP*, 115, 928
- Kennicutt, Jr., R. C., Calzetti, D., Walter, F., et al. 2007, *ApJ*, 671, 333
- Kepley, A. A., Leroy, A. K., Frayer, D., et al. 2014, *ApJ*, 780, L13
- Kewley, L. J., & Dopita, M. A. 2002, *ApJS*, 142, 35
- Knapp, G. R., & Bowers, P. F. 1988, *ApJ*, 331, 974
- Kobulnicky, H. A., & Kewley, L. J. 2004, *ApJ*, 617, 240
- Koda, J., Scoville, N., Sawada, T., et al. 2009, *ApJ*, 700, L132
- Komugi, S., Kohno, K., Tosaki, T., et al. 2007, *PASJ*, 59, 55
- Kuno, N., Sato, N., Nakanishi, H., et al. 2007, *PASJ*, 59, 117
- Lada, C. J., Forbrich, J., Lombardi, M., & Alves, J. F. 2012, *ApJ*, 745, 190
- Leroy, A. K., Walter, F., Brinks, E., et al. 2008, *AJ*, 136, 2782
- Leroy, A. K., Walter, F., Sandstrom, K., et al. 2013, *AJ*, 146, 19
- Liu, G., Koda, J., Calzetti, D., Fukuhara, M., & Momose, R. 2011, *ApJ*, 735, 63
- Liu, L., Gao, Y., & Greve, T. R. 2015, *ApJ*, 805, 31
- Lynds, C. R., & Sandage, A. R. 1963, *ApJ*, 137, 1005
- Madsen, G. J., Reynolds, R. J., & Haffner, L. M. 2006, *ApJ*, 652, 401
- Mao, R.-Q., Schulz, A., Henkel, C., et al. 2010, *ApJ*, 724, 1336
- Martig, M., Crocker, A. F., Bounaud, F., et al. 2013, *MNRAS*, 432, 1914
- McGaugh, S. S. 1991, *ApJ*, 380, 140
- Meidt, S. E. 2016, *ApJ*, 818, 69
- Minamidani, T., Mizuno, N., Mizuno, Y., et al. 2008, *ApJS*, 175, 485
- Miura, R. E., Kohno, K., Tosaki, T., et al. 2012, *ApJ*, 761, 37
- . 2014, *ApJ*, 788, 167
- Momose, R., Okumura, S. K., Koda, J., & Sawada, T. 2010, *ApJ*, 721, 383
- Momose, R., Koda, J., Kennicutt, Jr., R. C., et al. 2013, *ApJ*, 772, L13
- Morokuma-Matsui, K., Sorai, K., Watanabe, Y., & Kuno, N. 2015, *PASJ*, 67, 2
- Moustakas, J., Kennicutt, Jr., R. C., Tremonti, C. A., et al. 2010, *ApJS*, 190, 233
- Muraoka, K., Kohno, K., Tosaki, T., et al. 2007, *PASJ*, 59, 43
- . 2009, *ApJ*, 706, 1213
- Muraoka, K., Takeda, M., Yanagitani, K., et al. 2016, *PASJ*, 68, 18
- Narayanan, D., Groppi, C. E., Kulesa, C. A., & Walker, C. K. 2005, *ApJ*, 630, 269
- Onodera, S., Kuno, N., Tosaki, T., et al. 2010, *ApJ*, 722, L127
- Pettini, M., & Pagel, B. E. J. 2004, *MNRAS*, 348, L59
- Pety, J., Schinnerer, E., Leroy, A. K., et al. 2013, *ApJ*, 779, 43
- Pierce, M. J. 1994, *ApJ*, 430, 53
- Pilyugin, L. S., & Thuan, T. X. 2005, *ApJ*, 631, 231
- Polk, K. S., Knapp, G. R., Stark, A. A., & Wilson, R. W. 1988, *ApJ*, 332, 432
- Rahman, N., Bolatto, A. D., Wong, T., et al. 2011, *ApJ*, 730, 72
- Rahman, N., Bolatto, A. D., Xue, R., et al. 2012, *ApJ*, 745, 183
- Roberts, W. W. 1969, *ApJ*, 158, 123
- Roman-Duval, J., Heyer, M., Brunt, C. M., et al. 2016, *ApJ*, 818, 144
- Rosolowsky, E. 2005, *PASP*, 117, 1403
- Rosolowsky, E., Keto, E., Matsushita, S., & Willner, S. P. 2007, *ApJ*, 661, 830
- Saha, A., Sandage, A., Tammann, G. A., et al. 1999, *ApJ*, 522, 802
- Sakamoto, K., Okumura, S. K., Ishizuki, S., & Scoville, N. Z. 1999, *ApJ*, 525, 691
- Sawada, T., Hasegawa, T., & Koda, J. 2012a, *ApJ*, 759, L26
- Sawada, T., Hasegawa, T., Sugimoto, M., Koda, J., & Handa, T. 2012b, *ApJ*, 752, 118
- Schruba, A., Leroy, A. K., Walter, F., et al. 2011, *AJ*, 142, 37
- Sheth, K., Vogel, S. N., Regan, M. W., et al. 2002, *AJ*, 124, 2581
- Shetty, R., Clark, P. C., & Klessen, R. S. 2014a, *MNRAS*, 442, 2208
- Shetty, R., Kelly, B. C., & Bigiel, F. 2013, *MNRAS*, 430, 288
- Shetty, R., Kelly, B. C., Rahman, N., et al. 2014b, *MNRAS*, 437, L61
- Shu, F. H., Milione, V., & Roberts, Jr., W. W. 1973, *ApJ*, 183, 819
- Solomon, P. M., Downes, D., & Radford, S. J. E. 1992, *ApJ*, 387, L55
- Su, Y.-N., Liu, S.-Y., Chen, H.-R., Zhang, Q., & Cesaroni, R. 2007, *ApJ*, 671, 571
- Takahashi, S., Saito, M., Ohashi, N., et al. 2008, *ApJ*, 688, 344
- Takeuchi, T. T., Yoshikawa, K., & Ishii, T. T. 2000, *ApJS*, 129, 1
- Tanaka, A., Nakanishi, H., Kuno, N., & Hirota, A. 2014, *PASJ*, 66, 66
- Thilker, D. A., Braun, R., & Walterbos, R. A. M. 2000, *AJ*, 120, 3070
- Thilker, D. A., Boissier, S., Bianchi, L., et al. 2007, *ApJS*, 173, 572
- Thim, F., Tammann, G. A., Saha, A., et al. 2003, *ApJ*, 590, 256
- Usero, A., Leroy, A. K., Walter, F., et al. 2015, *AJ*, 150, 115
- Utomo, D., Blitz, L., Davis, T., et al. 2015, *ApJ*, 803, 16
- van Kempen, T. A., Hogerheijde, M. R., van Dishoeck, E. F., et al. 2006, *A&A*, 454, L75
- Verley, S., Corbelli, E., Giovanardi, C., & Hunt, L. K. 2010, *A&A*, 510, A64
- Wada, K. 1994, *PASJ*, 46, 165
- Wada, K., Baba, J., & Saitoh, T. R. 2011, *ApJ*, 735, 1
- Wada, K., & Habe, A. 1992, *MNRAS*, 258, 82
- Walter, F., Brinks, E., de Blok, W. J. G., et al. 2008, *AJ*, 136, 2563
- Wilson, C. D., & Walker, C. E. 1994, *ApJ*, 432, 148
- Wilson, C. D., Warren, B. E., Israel, F. P., et al. 2009, *ApJ*, 693, 1736
- . 2012, *MNRAS*, 424, 3050
- Wu, J., Evans, II, N. J., Gao, Y., et al. 2005, *ApJ*, 635, L173
- Yao, L., Seaquist, E. R., Kuno, N., & Dunne, L. 2003, *ApJ*, 588, 771
- Young, J. S., & Sanders, D. B. 1986, *ApJ*, 302, 680
- Zaritsky, D., Kennicutt, Jr., R. C., & Huchra, J. P. 1994, *ApJ*, 420, 87